Hybrid Soft-Rigid Space Manipulators for On-Orbit Servicing

Lorenzo Ticozzi, Patricio A. Vela, Panagiotis Tsiotras

***Abstract*— This work introduces a novel hybrid soft-rigid spacecraft manipulator system (HSMS) integrating a tendon-driven continuum robot with a conventional satellite-mounted rigid manipulator. Building upon the Geometric Variable Strain (GVS) approach, the dynamic model of the HSMS is explicitly obtained as a set of minimal-order ordinary differential equations. Preliminary control design is conducted leveraging the obtained model, and a tracking maneuver is performed in simulation for the combined spacecraft-manipulator system. Numerical results are reported demonstrating the validity of the proposed approach and motivating further investigation in this problem.**

I. INTRODUCTION

Space manipulators, defined as spacecraft equipped with one or more robotic arms on the primary platform, will play a crucial role in various space-based scenarios, such as spacecraft servicing, in-space assembly, and manufacturing [1]. Despite the technological maturity demonstrated by past missions [2], [3], many challenges remain regarding autonomous operational capabilities [4], [5].

Most studies to date have focused on modeling and controlling rigid space manipulator platforms—systems comprising rigid bodies interconnected by rigid joints [6]-[9]. More recently, structural flexibility has been incorporated into system analysis and control design methodologies [10]-[12]. In the past few years, increasing attention has been dedicated to integrating soft robotics concepts into space-based applications [13], [14]. Soft robots are inherently lightweight and compliant [15], making them promising candidates for delicate space tasks such as dynamic grasping and in-space manipulation.

In this work, we build on recent advances to introduce a hybrid soft–rigid space manipulator system (HSMS) integrating a tendon-driven continuum link with a spacecraft-mounted rigid arm. Inspired by progress in modeling hybrid systems [19], [20], [26], we derive a compact, minimal-order set of ordinary differential equations that is particularly suitable for control design. To illustrate its effectiveness, we investigate a task-space controller that guides the soft link's tip along a challenging 3D trajectory, demonstrating excellent performance and motivating further developments.

This work has been supported by AFOSR award no. FA9550-23-1-0723.

Lorenzo Ticozzi and Panagiotis Tsiotras are with the D. Guggenheim School of Aerospace Engineering, Georgia Institute of Technology, Atlanta, GA 30332-0150, USA. {lorenzo, tsiotras}@gatech.edu

Patricio A. Vela is with the Department of Electrical and Computer Engineering, Georgia Institute of Technology, Atlanta, GA 30332-0150, USA. pvela@gatech.edu

II. HYBRID SPACE MANIPULATOR MODEL

In this section, we introduce the mathematical notation used throughout the paper, followed by the kinematic and dynamic models of the hybrid soft–rigid spacecraft–manipulator system (HSMS). For clarity, we focus on a representative configuration in which a satellite-mounted, 2-DoF rigid manipulator with revolute joints carries a tendon-driven continuum link, as shown in Fig. 1. However, the proposed formulation generalizes to any interconnection of rigid and soft links mounted on a free-flying base.

A. Notation and HSMS Kinematics

We denote the pose transformation from frame $\mathcal{Y}$ to frame $\mathcal{Z}$ by $\boldsymbol{g}_{\mathcal{Y}/\mathcal{Z}} \in \mathrm{SE}(3)$, where $\mathrm{SE}(3)$ is the special Euclidean group. Vectors in $\mathfrak{se}(3)$, the Lie algebra of $\mathrm{SE}(3)$, also play a key role in our exposition. Depending on the context, we refer to these vectors either by their coordinate representation in $\mathbb{R}^6$ or as elements of $\mathfrak{se}(3)$. The "hat" symbol $\hat{\cdot}$ denotes the isomorphism $\hat{(\cdot)} : \mathbb{R}^6 \to \mathfrak{se}(3)$. The Adjoint representation $\mathrm{Ad}_{\boldsymbol{g}}(\cdot) : \mathfrak{se}(3) \to \mathfrak{se}(3)$ encodes a coordinate transformation between different frames, while the Lie algebra adjoint $\mathrm{ad}_{\boldsymbol{\xi}}(\cdot) : \mathfrak{se}(3) \to \mathfrak{se}(3)$ arises from differentiating $\mathrm{Ad}_{\boldsymbol{g}}$ with respect to $\boldsymbol{g}$. For further details, see [17] and Appendix A in [16].

Consider the schematic of the HSMS in Fig. 1. We define an inertial reference frame $\mathcal{I}$, along with a spacecraft-base frame $\mathcal{B}$ located at the base's center of mass, whose axes align with the base's principal inertia axes. Two additional frames, $\mathcal{R}_1$, $\mathcal{R}_2$, are assigned to the rigid manipulator links in the same manner. The root of the soft link is attached at the end of the second link, and the curvilinear coordinate $s \in [0, \ell]$ spans its continuum backbone from root ($s = 0$) to tip ($s = \ell$). A cross-sectional frame $\mathcal{X}(s)$ is associated with each cross-section of the soft link at coordinate s. For convenience, we define two further frames at the root and tip of the soft link: $\mathcal{F} \triangleq \mathcal{X}(s = 0)$ and $\mathcal{E} \triangleq \mathcal{X}(s = l)$.

Referring to Fig. 1, the pose of frame $\mathcal{F}$ with respect to frame $\mathcal{I}$ is given by

$$\boldsymbol{g}_{\mathcal{I}/\mathcal{F}}(\boldsymbol{q}_R) = \boldsymbol{g}_{\mathcal{I}/\mathcal{B}}(\boldsymbol{q}_B)\boldsymbol{g}_{\mathcal{B}/\mathcal{R}_1}(q_1)\boldsymbol{g}_{\mathcal{R}_1/\mathcal{R}_2}(q_2)\boldsymbol{g}_{\mathcal{R}_2/\mathcal{F}}, \quad (1)$$

where $\boldsymbol{q}_R \triangleq [\boldsymbol{q}_B, q_1, q_2]^\intercal$, with $\boldsymbol{q}_B \in \mathbb{R}^6$ representing the base degrees of freedom, and scalars q_1, q_2 denoting the joint angles. The configuration of the soft appendage is described by a curve in $\mathrm{SE}(3)$, $\boldsymbol{g}_{F/X}(\cdot) : [0, \ell] \to \mathrm{SE}(3)$, where $\boldsymbol{g}_{F/E} = \boldsymbol{g}_{F/X}(s = \ell)$. Consequently, the pose of the end-effector frame $\mathcal{E}$ with respect to $\mathcal{I}$ is

$$\boldsymbol{g}_{\mathcal{I}/\mathcal{E}} = \boldsymbol{g}_{\mathcal{I}/\mathcal{F}}(\boldsymbol{q}_R)\boldsymbol{g}_{\mathcal{F}/\mathcal{E}}. \quad (2)$$

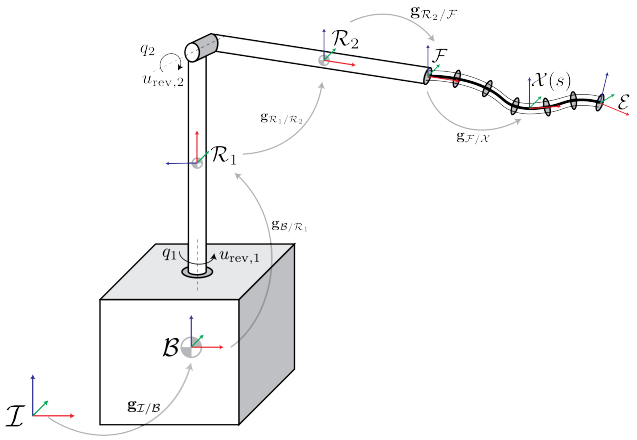

Fig. 1: Schematic of the HSMS platform.

According to [19], the relationship between $\boldsymbol{g}(s)$ and the strain field $\hat{\boldsymbol{\xi}}(s)$ is given by

$$\hat{\boldsymbol{\xi}}(s) = \boldsymbol{g}^{-1}(s)\boldsymbol{g}'(s), \quad \hat{\boldsymbol{\xi}}(s) \in \mathfrak{se}(3), \tag{3}$$

where $(\cdot)' \triangleq \partial/\partial s(\cdot)$. Similarly, the velocity field $\hat{\boldsymbol{\eta}}(s) \in \mathfrak{se}(3)$, also referred to as body twist, is defined as

$$\hat{\boldsymbol{\eta}}(s) = \boldsymbol{g}^{-1}(s)\dot{\boldsymbol{g}}(s), \tag{4}$$

with $\dot{(\cdot)} \triangleq \partial/\partial t(\cdot)$.

From Eq. (4), the end-effector twist can be written as

$$\hat{\boldsymbol{\eta}}^{\mathcal{E}}_{\mathcal{I}/\mathcal{E}} = \boldsymbol{g}^{-1}_{\mathcal{I}/\mathcal{E}}\dot{\boldsymbol{g}}_{\mathcal{I}/\mathcal{E}}, \tag{5}$$

where, in general, vector $\boldsymbol{\eta}^{\mathcal{Z}}_{\mathcal{X}/\mathcal{Y}} \in \mathbb{R}^6$ is read as "the velocity components of frame $\mathcal{Y}$ with respect to frame $\mathcal{X}$, expressed in frame $\mathcal{Z}$". In what follows, when the superscript is omitted, assume $\mathcal{Z} \equiv \mathcal{Y}$. Substituting Eqs. (1) and (2) into Eq. (5) and transforming the twists by means of the Adjoint, we obtain

$$\boldsymbol{\eta}_{\mathcal{I}/\mathcal{E}} = \mathrm{Ad}_{\boldsymbol{g}^{-1}_{\mathcal{B}/\mathcal{E}}}(\boldsymbol{\eta}_{\mathcal{I}/\mathcal{B}}) + \cdots + \mathrm{Ad}_{\boldsymbol{g}^{-1}_{\mathcal{R}_2/\mathcal{E}}}(\boldsymbol{\eta}_{\mathcal{R}_1/\mathcal{R}_2}) + \boldsymbol{\eta}_{\mathcal{F}/\mathcal{E}}. \tag{6}$$

Although Eq. (6) expresses the end-effector twist as the sum of the system's body velocities with respect to their parent frames, we seek a more convenient relationship involving only the base velocity, the rigid-link joint rates, and the strain field rate $\dot{\hat{\boldsymbol{\xi}}}(s)$. In a purely rigid manipulator, the joint velocities are linearly mapped to the end-effector's Cartesian velocity through the end-effector Jacobian (see Chapter 3 in [16]). Therefore, the twist coordinates in Eq. (6) can also be obtained as

$$\boldsymbol{\eta}_{\mathcal{I}/\mathcal{E}} = \boldsymbol{J}^{\mathcal{E}}_R(\boldsymbol{q}_R)\dot{\boldsymbol{q}}_R + \boldsymbol{\eta}_{\mathcal{F}/\mathcal{E}}. \tag{7}$$

A few additional steps are needed to express $\boldsymbol{\eta}_{\mathcal{F}/\mathcal{E}}$ in terms of the strain field rate, whose detailed explanation can be found in [18]. In summary, after stating the following compatibility equation at the strain and velocity level,

$$\hat{\boldsymbol{\eta}}' = \dot{\hat{\boldsymbol{\xi}}} - \mathrm{ad}_{\hat{\boldsymbol{\xi}}}(\hat{\boldsymbol{\eta}}), \tag{8}$$

an expression for $\hat{\boldsymbol{\eta}}(s)$ can be found by analytical integration of Eq. (8),

$$\hat{\boldsymbol{\eta}}(s) = \mathrm{Ad}^{-1}_{\boldsymbol{g}(s)}\left(\int_0^s \mathrm{Ad}_{\boldsymbol{g}(\sigma)}\big(\dot{\hat{\boldsymbol{\xi}}}(\sigma)\big)\mathrm{d}\sigma\right). \tag{9}$$

Since the strain field $\hat{\boldsymbol{\xi}}(s)$ is infinite dimensional, in order to make the problem tractable, the following approximation of the strain field by means of a set of basis functions $\boldsymbol{\Phi}_{\boldsymbol{\xi}}$ has been proposed,

$$\boldsymbol{\xi}(s, \boldsymbol{q}_S) = \boldsymbol{\Phi}_{\boldsymbol{\xi}}(s)\boldsymbol{q}_S + \boldsymbol{\xi}^*(s), \tag{10}$$

where $\boldsymbol{\Phi}_{\boldsymbol{\xi}} : \mathbb{R} \mapsto \mathbb{R}^{6\times S}$ is a function of the arc-length coordinate, $\boldsymbol{q}_S \in \mathbb{R}^S$ is a finite-dimensional vector of discretizing coordinates, and $\boldsymbol{\xi}^*(s)$ is a reference strain state. The approximation in Eq. (10) underpins the approach known as Geometric Variable Strain (GVS) (see [19], [20], [21]). Inserting Eq. (10) into Eq. (9) and letting $\boldsymbol{\xi}^* = \boldsymbol{0}$, we obtain

$$\boldsymbol{\eta}(s) = \mathrm{Ad}^{-1}_{\boldsymbol{g}(s)}\int_0^s \mathrm{Ad}_{\boldsymbol{g}(\sigma)}\boldsymbol{\Phi}_{\boldsymbol{\xi}}(\sigma)\mathrm{d}\sigma\,\dot{\boldsymbol{q}}_S, \tag{11}$$

in which the right hand side can be approximated, for example, with a quadrature method. Plugging Eq. (11) into Eq. (6) yields

$$\begin{aligned}\boldsymbol{\eta}_{\mathcal{I}/\mathcal{E}} &= \boldsymbol{J}^{\mathcal{E}}_R(\boldsymbol{q}_R)\dot{\boldsymbol{q}}_R + \mathrm{Ad}^{-1}_{\boldsymbol{g}_{\mathcal{F}/\mathcal{E}}}\int_0^\ell \mathrm{Ad}_{\boldsymbol{g}_{\mathcal{F}/\mathcal{X}}}\boldsymbol{\Phi}_{\boldsymbol{\xi}}(s)\,\mathrm{d}s\dot{\boldsymbol{q}}_S &(12)\\ &= \boldsymbol{J}^{\mathcal{E}}_R(\boldsymbol{q}_R)\dot{\boldsymbol{q}}_R + \boldsymbol{J}^{\mathcal{E}}_S(\boldsymbol{q}_S)\dot{\boldsymbol{q}}_S &(13)\\ &= \boldsymbol{J}^{\mathcal{E}}(\boldsymbol{q})\dot{\boldsymbol{q}}, &(14)\end{aligned}$$

where $\boldsymbol{q} = \left[\boldsymbol{q}_R^\mathsf{T}, \boldsymbol{q}_S^\mathsf{T}\right]^\mathsf{T} \in \mathbb{R}^{n=6+R+S}$, $\boldsymbol{J}^{\mathcal{E}} \triangleq [\boldsymbol{J}^{\mathcal{E}}_R, \boldsymbol{J}^{\mathcal{E}}_S]$, and we have defined the soft end-effector Jacobian as follows,

$$\boldsymbol{J}^{\mathcal{E}}_S \triangleq \mathrm{Ad}^{-1}_{\boldsymbol{g}_{\mathcal{F}/\mathcal{E}}}\int_0^\ell \mathrm{Ad}_{\boldsymbol{g}_{\mathcal{F}/\mathcal{X}}}\boldsymbol{\Phi}_{\boldsymbol{\xi}}(s)\,\mathrm{d}s. \tag{15}$$

Note that a further acceleration-level relationship can be constructed by differentiating Eq. (14) (see details in [18]),

$$\dot{\boldsymbol{\eta}}_{\mathcal{I}/\mathcal{E}} = \dot{\boldsymbol{J}}^{\mathcal{E}}(\boldsymbol{q}, \dot{\boldsymbol{q}})\dot{\boldsymbol{q}} + \boldsymbol{J}^{\mathcal{E}}(\boldsymbol{q})\ddot{\boldsymbol{q}}. \tag{16}$$

B. HSMS Dynamics

Building upon the kinematic model presented in Section II-A, the dynamic model of the HSMS can be derived by applying the D'Alembert's form of the principle of virtual work (PVW).

To this end, consider the j-th rigid body within the HSMS, for which momentum variation equals the net applied wrench, as follows,

$$\frac{\partial}{\partial t}\boldsymbol{\ell}^{\mathcal{I}}_j = \boldsymbol{w}^{\mathcal{I}}_j. \tag{17}$$

In Eq. (17), $\boldsymbol{\ell}^{\mathcal{I}}_j = \boldsymbol{M}_j\boldsymbol{\eta}^{\mathcal{I}}_{\mathcal{I}/j}$ is the body momentum, $\boldsymbol{M}_j$ is the constant body inertia matrix, and $\boldsymbol{w}^{\mathcal{I}}_j$ is the net wrench acting on j. We expand the net wrench as $\boldsymbol{w}^{\mathcal{I}}_j = \boldsymbol{w}^{\mathcal{I}}_{j,e} + \boldsymbol{w}^{\mathcal{I}}_{j,a} + \boldsymbol{w}^{\mathcal{I}}_{j,c}$, where $\boldsymbol{w}^{\mathcal{I}}_{j,e}, \boldsymbol{w}^{\mathcal{I}}_{j,a}, \boldsymbol{w}^{\mathcal{I}}_{j,c}$ denote the wrenches due to external factors, to the actuation and to the constraints, respectively. Then, after applying the coordinate transformations $\boldsymbol{\ell}^{\mathcal{I}}_j =$

$\mathrm{Ad}^*_{\boldsymbol{g}_{\mathcal{I}/j}}\boldsymbol{\ell}_j$ and $\boldsymbol{w}_j^{\mathcal{I}} = \mathrm{Ad}^*_{\boldsymbol{g}_{\mathcal{I}/j}}\boldsymbol{w}_j$, Eq. (17) can be rewritten in the j-th body coordinates,

$$\boldsymbol{M}_j\dot{\boldsymbol{\eta}}_{\mathcal{I}/j} + \mathrm{ad}^*_{\boldsymbol{\eta}_{\mathcal{I}/j}}\boldsymbol{M}_j\boldsymbol{\eta}_{\mathcal{I}/j} = \boldsymbol{w}_{j,e} + \boldsymbol{w}_{j,a} + \boldsymbol{w}_{j,c}. \quad (18)$$

The dynamic equilibrium for the cross-sectional frame $\mathcal{X}$ along the soft link has a similar formulation [18],

$$\bar{\boldsymbol{M}}_{\mathcal{X}}\dot{\boldsymbol{\eta}}_{\mathcal{I}/\mathcal{X}} + \mathrm{ad}^*_{\boldsymbol{\eta}_{\mathcal{I}/\mathcal{X}}}\bar{\boldsymbol{M}}_{\mathcal{X}}\boldsymbol{\eta}_{\mathcal{I}/\mathcal{X}} = (\boldsymbol{\mu} - \boldsymbol{w}_{\mathcal{X},a})' + \mathrm{ad}^*_{\boldsymbol{\xi}}(\boldsymbol{\mu} - \boldsymbol{w}_{\mathcal{X},a}) + \bar{\boldsymbol{w}}_{\mathcal{X},e}, \quad (19)$$

where $\bar{\boldsymbol{M}}_{\mathcal{X}}$ is the cross-section inertia matrix, $\boldsymbol{\mu}$ is the internal wrench, $\boldsymbol{w}_{\mathcal{X},a}$ is the wrench provided by the soft actuators and $\bar{\boldsymbol{w}}_{\mathcal{X},e}$ is the net external load per unit of material length.

Let us recall D'Alembert's formulation of the PVW [22], written as

$$\delta W = \delta W_{\text{int}} - \delta W_{\text{ext}} = 0, \quad (20)$$

where δW_{int} and δW_{ext} denote the total internal and external virtual work, respectively. Within the HSMS, the internal virtual work is performed by the internal wrench $\boldsymbol{\mu}$ and by the soft actuation wrench $\boldsymbol{w}_{\mathcal{X},a}$ acting along a compatible variation of the strain, denoted as $\delta\boldsymbol{\xi}$,

$$\delta W_{\text{int}} = \int_0^\ell \delta\boldsymbol{\xi}\cdot(\boldsymbol{\mu} - \boldsymbol{w}_{\mathcal{X},a})\,\mathrm{d}s. \quad (21)$$

The total external virtual work is accomplished by the body loads and by the inertial forces introduced in Eqs. (18) and (19),

$$\delta W_{\text{ext}} = \delta\boldsymbol{r}_{\mathcal{B}}\cdot\boldsymbol{f}_{\mathcal{B}} + \sum_{i=1,2}\delta\boldsymbol{r}_{\mathcal{R}_i}\cdot\boldsymbol{f}_{\mathcal{R}_i} + \int_0^\ell \delta\boldsymbol{r}_{\mathcal{X}}\cdot\boldsymbol{f}_{\mathcal{X}}\,\mathrm{d}s, \quad (22)$$

where $\delta\boldsymbol{r}_{\mathcal{B}}, \delta\boldsymbol{r}_{\mathcal{R}_i}$ and $\delta\boldsymbol{r}_{\mathcal{X}}$ denote the virtual displacements, and the following quantities have been defined,

$$\boldsymbol{f}_{\mathcal{B}} \triangleq \boldsymbol{w}_{\mathcal{B},e} + \boldsymbol{w}_{\mathcal{B},a} - (\boldsymbol{M}_{\mathcal{B}}\dot{\boldsymbol{\eta}}_{\mathcal{I}/\mathcal{B}} + \mathrm{ad}^*_{\boldsymbol{\eta}_{\mathcal{I}/\mathcal{B}}}\boldsymbol{M}_{\mathcal{B}}\boldsymbol{\eta}_{\mathcal{I}/\mathcal{B}}), \quad (23)$$

$$\boldsymbol{f}_{\mathcal{R}_i} \triangleq \boldsymbol{w}_{\mathcal{R}_i,e} + \boldsymbol{w}_{\mathcal{R}_i,a} - (\boldsymbol{M}_{\mathcal{R}_i}\dot{\boldsymbol{\eta}}_{\mathcal{I}/\mathcal{R}_i} \quad (24)$$

$$+ \mathrm{ad}^*_{\boldsymbol{\eta}_{\mathcal{I}/\mathcal{R}_i}}\boldsymbol{M}_{\mathcal{R}_i}\boldsymbol{\eta}_{\mathcal{I}/\mathcal{R}_i}), \quad (25)$$

$$\boldsymbol{f}_{\mathcal{X}} \triangleq \bar{\boldsymbol{w}}_{\mathcal{X},e} - (\bar{\boldsymbol{M}}_{\mathcal{X}}\dot{\boldsymbol{\eta}}_{\mathcal{I}/\mathcal{X}} + \mathrm{ad}^*_{\boldsymbol{\eta}_{\mathcal{I}/\mathcal{X}}}\bar{\boldsymbol{M}}_{\mathcal{X}}\boldsymbol{\eta}_{\mathcal{I}/\mathcal{X}}). \quad (26)$$

Note that the constraint reaction forces do not contribute to the work performed during any admissible virtual displacement.

To obtain the equations of motion, the virtual displacements in Eqs. (21) and (22) need to be expressed in terms of the system's generalized coordinates,

$$\delta\boldsymbol{\xi} = \hat{\boldsymbol{\Phi}}_{\boldsymbol{\xi}}\delta\boldsymbol{q},\ \delta\boldsymbol{r}_{\mathcal{B}} = \boldsymbol{J}^{\mathcal{B}}\delta\boldsymbol{q},\ \delta\boldsymbol{r}_{\mathcal{R}_i} = \boldsymbol{J}^{\mathcal{R}_i}\delta\boldsymbol{q},\ \delta\boldsymbol{r}_{\mathcal{X}} = \boldsymbol{J}^{\mathcal{X}}\delta\boldsymbol{q}, \quad (27)$$

where $\hat{\boldsymbol{\Phi}}_{\boldsymbol{\xi}}, \boldsymbol{J}^{\mathcal{B}}, \boldsymbol{J}^{\mathcal{R}_i}, \boldsymbol{J}^{\mathcal{X}}$ project $\delta\boldsymbol{q}$ onto the relevant displacement. With additional (omitted) steps, the system's velocities and accelerations are also obtained in terms of $\boldsymbol{q}, \dot{\boldsymbol{q}}$, and $\ddot{\boldsymbol{q}}$. After carrying out the necessary substitutions in Eqs.(23)-(26) as well as in the expressions of δW_{int} (Eq. (21)) and δW_{ext} (Eq. (22)), the PVW equality in Eq. (20) is applied and rearranged to yield the following compact form of the HSMS dynamics:

$$\boldsymbol{M}(\boldsymbol{q})\ddot{\boldsymbol{q}} + \boldsymbol{C}(\boldsymbol{q},\dot{\boldsymbol{q}})\dot{\boldsymbol{q}} + \boldsymbol{K}(\boldsymbol{q})\boldsymbol{q} = \boldsymbol{W}_{\text{ext}}(\boldsymbol{q}) + \boldsymbol{B}(\boldsymbol{q})\boldsymbol{u}. \quad (28)$$

Here, $\boldsymbol{M} \in \mathbb{R}^{n\times n}$ is the generalized inertia matrix, $\boldsymbol{C} \in \mathbb{R}^{n\times n}$ contains the nonlinear velocity terms, $\boldsymbol{K} \in \mathbb{R}^{n\times n}$ originates from the elastic deformation of the soft link, $\boldsymbol{W}_{\text{ext}} \in \mathbb{R}^n$ describes the effect of the applied external wrenches and $\boldsymbol{B} \in \mathbb{R}^{n\times m}$ maps the actuation inputs $\boldsymbol{u} \in \mathbb{R}^m$ onto the configuration space.

It is noteworthy that, unlike current results for spacecraft-mounted continuum manipulators (e.g., [23]-[25]), the HSMS dynamics in Eq. (28) are obtained as a compact set of minimum-order ODEs rather than as a high-dimensional system of differential-algebraic equations (DAEs). This is particularly useful when tackling control design for the combined HSMS system, as shown in the following section.

III. CONTROL DESIGN

In this section, we leverage the results from Section II to design a controller for the HSMS. Our main objective is to demonstrate how the proposed modeling approach greatly simplifies the control design for the system at hand. Hence, we focus on a relatively straightforward inverse-dynamics controller and leave the development of more advanced schemes for future work. In what follows, we assume that the external wrench acting on the system is negligible compared to the control action $\boldsymbol{u}$, and therefore consider $\boldsymbol{W}_{\text{ext}} = \boldsymbol{0}$.

Consider the problem of designing a control law such that the end-effector of the HSMS tracks a time-varying position $\boldsymbol{r}^{\mathcal{I}}_{\mathcal{I}/\mathcal{D}}(t)$, where $\mathcal{D}$ denotes a desired frame. To this end, we define a reference curve in $\mathrm{SE}(3)$, $\boldsymbol{g}_{\mathcal{I}/\mathcal{D}} : \mathbb{R} \to \mathrm{SE}(3)$,

$$\boldsymbol{g}_{\mathcal{I}/\mathcal{D}}(t) = \begin{bmatrix}\boldsymbol{R}_{\mathcal{I}/\mathcal{D}} & \boldsymbol{r}^{\mathcal{I}}_{\mathcal{I}/\mathcal{D}}(t)\\ \boldsymbol{0}_{1\times 3} & 1\end{bmatrix}, \quad (29)$$

where $\boldsymbol{R}_{\mathcal{I}/\mathcal{D}} \in \mathrm{SO}(3)$ is the attitude of the desired frame, considered constant for the sake of simplicity. Given $\boldsymbol{g}_{\mathcal{I}/\mathcal{D}}$, its time derivatives $\dot{\boldsymbol{g}}_{\mathcal{I}/\mathcal{D}}$ and $\ddot{\boldsymbol{g}}_{\mathcal{I}/\mathcal{D}}$ are easily computed. Then, the desired end-effector twist is obtained leveraging Eq. (4),

$$\hat{\boldsymbol{\eta}}^{\mathcal{E}}_{\mathcal{I}/\mathcal{D}} = \mathrm{Ad}_{\boldsymbol{g}_{\mathcal{E}/\mathcal{D}}}(\hat{\boldsymbol{\eta}}^{\mathcal{I}}_{\mathcal{I}/\mathcal{D}}) = \mathrm{Ad}_{\boldsymbol{g}_{\mathcal{E}/\mathcal{D}}}(\boldsymbol{g}^{-1}_{\mathcal{I}/\mathcal{D}}\dot{\boldsymbol{g}}_{\mathcal{I}/\mathcal{D}}), \quad (30)$$

from which the velocity error follows, $\hat{\boldsymbol{\eta}}^{\mathcal{E}}_{\mathcal{E}/\mathcal{D}} = \hat{\boldsymbol{\eta}}^{\mathcal{E}}_{\mathcal{I}/\mathcal{D}} - \hat{\boldsymbol{\eta}}^{\mathcal{E}}_{\mathcal{I}/\mathcal{E}}$. Note that the linear velocity of the end-effector expressed in the $\mathcal{E}$ frame is given by $\boldsymbol{v}^{\mathcal{E}}_{\mathcal{I}/\mathcal{E}} = \boldsymbol{J}^{\mathcal{E}}_l(\boldsymbol{q})\dot{\boldsymbol{q}}$, where $\boldsymbol{J}^{\mathcal{E}}_l$ is an appropriate partition of the Jacobian $\boldsymbol{J}^{\mathcal{E}}$. Finally, the time derivative of the desired end-effector twist is obtained by differentiating Eq. (30),

$$\dot{\hat{\boldsymbol{\eta}}}^{\mathcal{E}}_{\mathcal{I}/\mathcal{D}} = \mathrm{ad}_{\hat{\boldsymbol{\eta}}_{\mathcal{E}/\mathcal{D}}}\big(\mathrm{Ad}_{\boldsymbol{g}_{\mathcal{E}/\mathcal{D}}}(\hat{\boldsymbol{\eta}}_{\mathcal{I}/\mathcal{D}})\big) + \mathrm{Ad}_{\boldsymbol{g}_{\mathcal{E}/\mathcal{D}}}(\dot{\hat{\boldsymbol{\eta}}}_{\mathcal{I}/\mathcal{D}}). \quad (31)$$

Notice that the linear velocity error of the end effector, $\boldsymbol{v}^{\mathcal{E}}_{\mathcal{E}/\mathcal{D}} \in \mathbb{R}^3$, and its desired linear acceleration $\dot{\boldsymbol{v}}^{\mathcal{E}}_{\mathcal{I}/\mathcal{D}} \in \mathbb{R}^3$ are known since $\boldsymbol{\eta}^{\mathcal{E}}_{\mathcal{E}/\mathcal{D}} = \big[(\boldsymbol{\omega}^{\mathcal{E}}_{\mathcal{E}/\mathcal{D}})^{\intercal}, (\boldsymbol{v}^{\mathcal{E}}_{\mathcal{E}/\mathcal{D}})^{\intercal}\big]^{\intercal}$ and $\dot{\boldsymbol{\eta}}^{\mathcal{E}}_{\mathcal{I}/\mathcal{D}} = \big[(\dot{\boldsymbol{\omega}}^{\mathcal{E}}_{\mathcal{I}/\mathcal{D}})^{\intercal}, (\dot{\boldsymbol{v}}^{\mathcal{E}}_{\mathcal{I}/\mathcal{D}})^{\intercal}\big]^{\intercal}$.

Lemma 3.1: Consider the hybrid spacecraft manipulator system with dynamics described by Eq. (28), and let $\boldsymbol{r}^{\mathcal{I}}_{\mathcal{I}/\mathcal{D}}(t)$ be a desired position trajectory for the end-effector frame $\mathcal{E}$. The feedback control law

$$\boldsymbol{u} = \big(\boldsymbol{J}^{\mathcal{E}}_l\boldsymbol{M}^{-1}\boldsymbol{B}\big)^{\dagger}\big[\boldsymbol{\theta} + \boldsymbol{J}^{\mathcal{E}}_l\boldsymbol{M}^{-1}(\boldsymbol{C}\dot{\boldsymbol{q}} + \boldsymbol{K}\boldsymbol{q}) - \dot{\boldsymbol{J}}^{\mathcal{E}}_l\dot{\boldsymbol{q}}\big] \quad (32)$$

yields the following decoupled task-space dynamics,

$$\dot{\boldsymbol{v}}^{\mathcal{E}}_{\mathcal{I}/\mathcal{E}} = \boldsymbol{\theta}, \quad (33)$$

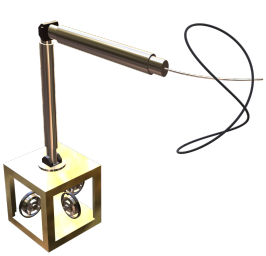

(a) HSMS configuration at $t = 0$ s.

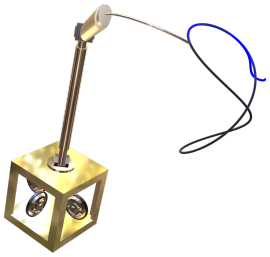

(b) HSMS configuration at $t = 100$ s.

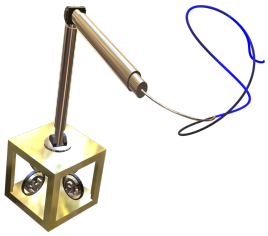

(c) HSMS configuration at $t = 200$ s.

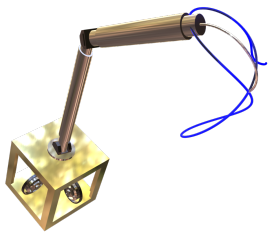

(d) HSMS configuration at $t = 300$ s.

Fig. 2: Snapshots of the tracking scenario. The blue curve denotes the end-effector trajectory throughout the maneuver, while the black one represents the desired end-effector path.

where $\boldsymbol{\theta}$ is an auxiliary control input. Moreover, if

$$\boldsymbol{\theta} = \dot{\boldsymbol{v}}^{\mathcal{E}}_{\mathcal{I}/\mathcal{D}} + \boldsymbol{K}_d \boldsymbol{v}^{\mathcal{E}}_{\mathcal{E}/\mathcal{D}} + \boldsymbol{K}_p \boldsymbol{r}^{\mathcal{E}}_{\mathcal{E}/\mathcal{D}}, \tag{34}$$

with $\boldsymbol{K}_d, \boldsymbol{K}_p \succ 0$, then $\lim_{t\to\infty} \boldsymbol{r}^{\mathcal{I}}_{\mathcal{I}/\mathcal{E}}(t) = \boldsymbol{r}^{\mathcal{I}}_{\mathcal{I}/\mathcal{D}}(t)$.

Proof: The proof follows the standard procedure showing asymptotic stability of a task-space inverse dynamics controller (see, e.g., Sec. 5.4 in [16]), and is therefore left to the reader. ■

IV. NUMERICAL RESULTS

The model and controller presented in the preceding sections have been implemented in MATLAB leveraging the SoRoSim library [26]. Our case study considers the system depicted in Fig. 1, whose main physical parameters are reported in Table I. The soft link has a Young's modulus of 10^6 N/m^2 and a Poisson's ratio equal to 0.5. Following the GVS approach introduced in Eq. (10), we choose to parameterize the y-axis bending of the soft appendage with a linear function, while the z-axis bending is described by a constant. Torsion, shear and extension are neglected. To increase realism in our simulations, we choose to actuate the base by means of thrusters and single-gimbal variable-speed control moment gyros (VSCMGs), following a similar approach to [27]. The rigid manipulator links are actuated by two revolute joints, while the soft link is actuated with three parallel tendons routed along the whole backbone length, whose coordinates in the cross-section frame $\mathcal{X}(s)$ are defined in meters as $\boldsymbol{d}_1(s) = [0, 0.05\cos(\pi/6), 0.05\sin(\pi/6)]^\intercal$, $\boldsymbol{d}_2(s) = [0, -0.05\cos(\pi/6), 0.05\sin(\pi/6)]^\intercal$ and $\boldsymbol{d}_3(s) = [0, 0, -0.05]^\intercal$.

TABLE I: Physical parameters of the hybrid spacecraft-manipulator system (HSMS).

Body	**Shape**	**Dimensions**, m	**Density**, kg/m^3
Base	Cube	Edge: 1	100
Rigid links	Cylinder	Radius: 0.1 Height: 2	100
Soft link	Cylinder	Radius: 0.01 Height: 1	1000

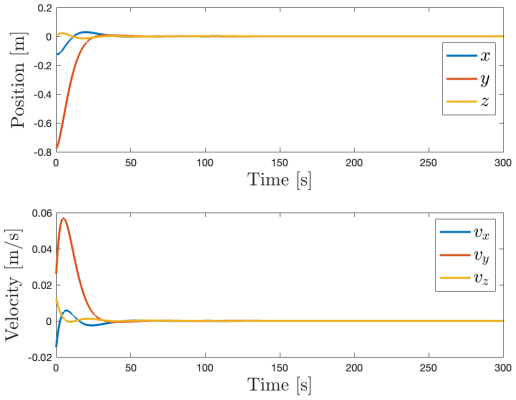

Fig. 3: End-effector position and velocity tracking error.

The end-effector is commanded to follow the so-called Viviani curve, specified as $\boldsymbol{r}^{\mathcal{I}}_{\mathcal{I}/\mathcal{D}}(t) = [\rho(1+\cos(\omega t)), \sin(\omega t), 2\sin(0.5\omega t)]^\intercal$, where $\rho = 0.3$ m and $\omega = 2\pi/T$, with $T = 150$ s. The controller gains in Eq. (34) are set to $\boldsymbol{K}_p = 0.03\boldsymbol{I}_3$ and $\boldsymbol{K}_d = 0.3\boldsymbol{I}_3$, where $\boldsymbol{I}_3$ is the identity matrix of dimension 3. In the interest of brevity, we only present a few snapshots of the tracking maneuver (Fig. 2), along with the corresponding tip position and linear velocity errors in Fig. 3. The error charts in Fig. 3 confirm that the proposed controller achieves excellent tracking performance. For better visualization, animations of the maneuver can be found at `https://youtu.be/kU00tmeFRSU`.

V. CONCLUSIONS

This paper formulates the dynamic model of a novel hybrid soft-rigid space manipulator system, leveraging geometric mechanics and the GVS methodology—a soft robotics approach that parametrizes continuum body strain via user-defined basis functions. The advantage of the proposed approach is demonstrated by the straightforward derivation and numerical implementation of a task-space tracking controller.

Overall, this work provides a first investigation of the modeling and control of hybrid soft–rigid space robotic platforms, which offer higher dexterity and operational flexibility compared to purely rigid systems. Many promising research directions remain open in terms of further analysis, control synthesis, and experimental validation of the proposed approach.

REFERENCES

[1] NASA Goddard Space Flight Center, "On-Orbit Satellite Servicing Study," 2010.

[2] Yoshida, K., "ETS-VII Flight Experiments For Space Robot Dynamics and Control," Experimental Robotics VII, edited by D. Rus and S. Singh, Springer Berlin, Berlin, 2001, pp. 209–218.

[3] Shoemaker, J., and Wright, M., "Orbital express space operations architecture program," Spacecraft Platforms and Infrastructure, Vol. 5419, edited by P. T. Jr. and M. Wright, International Society for Optics and Photonics, SPIE, 2004, pp. 57–65.

[4] Flores-Abad, A., Ma, O., Pham, K., and Ulrich, S., "A review of space robotics technologies for on-orbit servicing," Progress in Aerospace Sciences, Vol. 68, 2014, pp. 1–26.

[5] Papadopoulos, E., Aghili, F., Ma, O., and Lampariello, R., "Robotic Manipulation and Capture in Space: A Survey," Frontiers in Robotics and AI, Vol. 8, 2021.

[6] Dubowsky, S., and Papadopoulos, E., "The kinematics, dynamics, and control of free-flying and free-floating space robotic systems," IEEE Transactions on Robotics and Automation, Vol. 9, No. 5, 1993, pp. 531–543.

[7] Carignan, C., and Akin, D., "The reaction stabilization of on-orbit robots," IEEE Control Systems Magazine, Vol. 20, No. 6, 2000, pp. 19–33.

[8] Valverde, A., and Tsiotras, P., "Dual Quaternion Framework for Modeling of Spacecraft-Mounted Multibody Robotic Systems," Frontiers in Robotics and AI, Vol. 5, 2018.

[9] Seddaoui, A., Saaj, C. M., and Nair, M. H., "Modeling a Controlled-Floating Space Robot for In-Space Services: A Beginner's Tutorial," Frontiers in Robotics and AI, Vol. 8, 2021.

[10] Dubanchet, V., "Modeling and control of a flexible space robot to capture a tumbling debris," Ph.D. thesis, Ecole Polytechnique de Montreal, Canada, Jan. 2016.

[11] Zarafshan, P., and Moosavian, S. A. A., "Manipulation control of a space robot with flexible solar panels," 2010 IEEE/ASME International Conference on Advanced Intelligent Mechatronics, Montreal, Quebec, CA, 2010, pp. 1099–1104.

[12] Carabis, D. S., Oakes, K. I., and Wen, J. T., "Manipulation of Massive Objects in Space Using Flexible Joint Manipulators," Journal of Guidance, Control, and Dynamics, Vol. 44, No. 5, 2021, pp. 923–937.

[13] Li, K., Zhang, Y., and Hu, Q., "Dynamic modelling and control of a Tendon-Actuated Lightweight Space Manipulator," Aerospace Science and Technology, Vol. 84, 2019, pp. 1150–1163.

[14] Kernot, J. E., and Ulrich, S., "Adaptive Control of a Tendon-Driven Manipulator for Capturing Non-Cooperative Space Targets," Journal of Spacecraft and Rockets, Vol. 59, No. 1, 2022, pp. 111–128.

[15] Della Santina, C., Catalano, M. G., and Bicchi, A., Soft Robots, Springer Berlin Heidelberg, Berlin, Heidelberg, 2020, pp. 1–15.

[16] Murray, R. M., Li, Z., and Sastry, S. S., "A Mathematical Introduction to Robotic Manipulation," CRC Press, 1994.

[17] Marsden, J. E., and Ratiu, T. S., "Introduction to Mechanics and Symmetry," Texts in Applied Mathematics, Vol. 17, Springer New York, New York, 1999.

[18] Mathew, A. T., Feliu-Talegon, D., Alkayas, A. Y., Boyer, F., and Renda, F., "Reduced order modeling of hybrid soft-rigid robots using global, local, and state-dependent strain parameterization," The International Journal of Robotics Research, Vol. 44, No. 1, 2025, pp. 129–154.

[19] Renda, F., Armanini, C., Lebastard, V., Candelier, F., and Boyer, F., "A Geometric Variable-Strain Approach for Static Modeling of Soft Manipulators With Tendon and Fluidic Actuation," IEEE Robotics and Automation Letters, Vol. 5, No. 3, 2020, pp. 4006–4013.

[20] Boyer, F., Lebastard, V., Candelier, F., and Renda, F., "Dynamics of Continuum and Soft Robots: A Strain Parameterization Based Approach," IEEE Transactions on Robotics, Vol. 37, No. 3, 2021, pp. 847–863.

[21] Renda, F., Mathew, A., and Talegon, D. F., "Dynamics and Control of Soft Robots With Implicit Strain Parametrization," IEEE Robotics and Automation Letters, Vol. 9, No. 3, 2024, pp. 2782–2789.

[22] Reddy, J. N., An Introduction to Continuum Mechanics, 2nd ed., Cambridge University Press, 2013.

[23] Yang, J., Peng, H., Zhang, J., and Wu, Z., "Dynamic modeling and beating phenomenon analysis of space robots with continuum manipulators," Chinese Journal of Aeronautics, Vol. 35, No. 9, 2022, pp. 226–241.

[24] Yang, J., Peng, H., Zhou, W., and Wu, Z., "Integrated Control of Continuum-Manipulator Space Robots with Actuator Saturation and Disturbances," Journal of Guidance, Control, and Dynamics, Vol. 45, No. 12, 2022, pp. 2379–2388.

[25] Yang, J., Peng, H., Wu, S., Zhang, J., Wu, Z., and Wu, J., "Differential-algebraic equation-based model predictive control for trajectory tracking of spacecraft-mounted continuum manipulators," Aerospace Science and Technology, Vol. 155, 2024, Paper no. 109615.

[26] Mathew, A. T., Hmida, I. B., Armanini, C., Boyer, F., and Renda, F., "SoRoSim: A MATLAB Toolbox for Hybrid Rigid–Soft Robots Based on the Geometric Variable-Strain Approach," IEEE Robotics & Automation Magazine, Vol. 30, No. 3, 2023, pp. 106–122.

[27] Antonello, A., Valverde, A., and Tsiotras, P., "Dynamics and Control of Spacecraft Manipulators with Thrusters and Momentum Exchange Devices," Journal of Guidance, Control, and Dynamics, Vol. 42, No. 1, 2019, pp. 15–29.